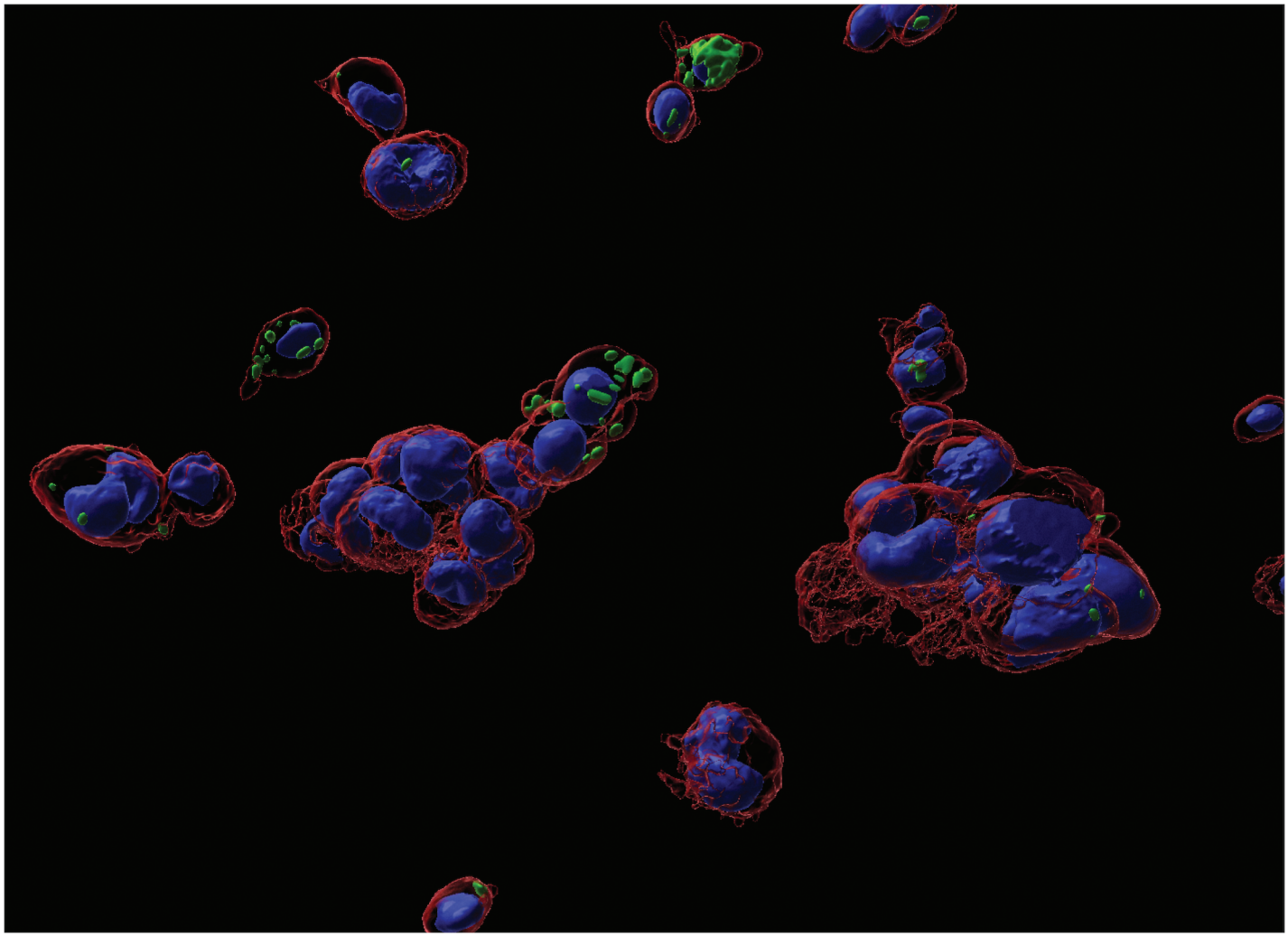

Showcasing research from Professor April Kloxin's laboratory, Chemical and Biomolecular Engineering, University of Delaware, USA.

High-throughput bioprinted 3D cultures for probing host–pathogen interactions in bioinspired microenvironments

Immune cells respond not only to pathogens and therapeutics, but also to the physical properties of their surrounding microenvironment in tissues within the human body. Our work develops high-throughput 3D biomaterial culture systems to study how immune cells respond to bacterial infection in tissue-like microenvironments. Using synthetic extracellular matrices printed with the RASTRUM bioprinter, we investigated macrophage responses to *Pseudomonas aeruginosa*. We observed differences in the magnitude of both bacterial clearance and inflammatory responses across matrices with fibrotic-like *versus* healthy-like stiffness, highlighting how microenvironment properties can shape early immune responses.

Image reproduced by permission of Jodi Graf from *RSC Appl. Polym.*, 2026, **4**, 543.

As featured in:

See Jodi Graf, DeVonte Moore *et al.*, *RSC Appl. Polym.*, 2026, **4**, 543.

ROYAL SOCIETY OF CHEMISTRY

rsc.li/RSCApplPolym

Registered charity number: 207890

RSC Applied Polymers

PAPER

View Article Online
View Journal | View Issue

Cite this: *RSC Appl. Polym.*, 2026, **4**, 543

High-throughput bioprinted 3D cultures for probing host–pathogen interactions in bioinspired microenvironments

Jodi Graf, *[a] DeVonte Moore, *[b] Catherine L. Grimes, †[b,c] Catherine A. Fromen †[a,d] and April M. Kloxin †[a,e]

The microenvironment of immune cells is an important regulator of their function and fate. Three-dimensional (3D) culture systems provide opportunities for probing immune cell responses to invading pathogens in microenvironments with biophysical and biochemical properties inspired by human tissues. Yet, the low throughput and manual preparation of many 3D culture models present challenges for translation of assays and their broad and accessible use for studying host–pathogen interactions. To address this, we established a high-throughput macrophage-bacteria co-culture model that mimics lung tissue stiffness across healthy and diseased conditions. Using bioprinting, human THP-1 monocytes were encapsulated and differentiated into macrophages within synthetic extracellular matrices (ECMs) fabricated with well-defined polymer and peptide bioinks in a 96-well plate format. Macrophages retained viability and displayed immunocompetence, including phenotype, phagocytosis, and response to stimuli. Macrophages in fibrosis-inspired 'stiffer' (storage modulus (G') ~4.8 kPa) microenvironments exhibited higher basal expression of both inflammation and traditional fibrosis associated genes compared to more compliant (G' ~1.1 kPa) synthetic ECMs inspired by healthy lung microenvironments. We applied our model 3D cultures to study immune response to invasion of a bacterial pathogen implicated in hospital born lung infections and mortality, *Pseudomonas aeruginosa*. Macrophages exhibited differential responses to *P. aeruginosa* in stiff microenvironments, with decreased cytokine secretion of IL-6 and IL-1β and elevated IL-10 and TNF-α compared to healthy compliant microenvironments, suggesting that microenvironment properties may shape initial immune responses. This high-throughput, accessible controlled platform provides opportunities for understanding human host–pathogen interactions and a foundation for identifying therapeutic strategies for bacterial infections in well-defined physiologically relevant microenvironments.

Received 11th September 2025,
Accepted 2nd January 2026

DOI: 10.1039/d5lp00285k

rsc.li/rscapplpolym

Introduction

Interactions between immune cells and pathogens are increasingly recognized as drivers of inflammation and disease.[1,2] The innate immune system provides fast, non-specific protection against a variety of foreign materials.[3] Macrophages, key innate immune cells found in tissues throughout the body, play essential roles in maintaining homeostasis and fighting infections.[4,5] As the first line of defense, macrophages detect, respond to, and eliminate foreign pathogens, particulates, and bacteria through phagocytosis (engulfment) and pro-inflammatory or anti-microbial signaling.[6–11] Invading pathogenic bacteria are responsible for complex host–pathogen interactions that involve immune evasion, hijacking immune cell machinery, and host cell death and can lead to a variety of diseases if untreated. First, invaders enter the body and are recognized by innate immune cells, primarily macrophages, through pathogen-associated molecular patterns (PAMPs) within the microbe, and then immune cells direct inflammatory processes against the foreign pathogens. This process often leads to resolution of the infection in healthy tissue microenvironments, yet can be unsuccessful in microenvironments with underlying disease, where mechanisms and how to target them are not fully understood.[12] While different *in vitro* systems (*e.g.*, organoid, microfluidic, scaffolds) have

[a]*Chemical and Biomolecular Engineering, University of Delaware, Newark, DE, USA. E-mail: cfromen@udel.edu, akloxin@udel.edu*
[b]*Chemistry and Biochemistry, University of Delaware, Newark, DE, USA. E-mail: cgrimes@udel.edu*
[c]*Biological Sciences, University of Delaware, Newark, DE, USA*
[d]*Biomedical Engineering, University of Delaware, Newark, DE, USA*
[e]*Material Science and Engineering, University of Delaware, Newark, DE, USA*
†Contributed equally.

been applied to studying these interactions,[13] most of what we know about host–pathogen interactions comes from traditional two-dimensional (2D) cultures on tissue-culture plastic (TCP) or mouse models.[8,14–17] Accessible and well-defined human three-dimensional (3D) culture systems, which can be easily and consistently used to probe how the immune system recognizes and responds to pathogens in physiologically relevant microenvironments, remain a need.

Macrophage phenotypes (*e.g.*, inflammatory (M1) or anti-inflammatory (M2)) are highly plastic and shift in response to external cues.[1,10,18,19] Further, macrophage functions are dependent on their microenvironment and are highly responsive to both biochemical and mechanical cues within the extracellular matrix (ECM). The ECM is a network of proteins and other bioactive cues that provided structure to our tissues and supports cellular function.[20,21] Several works have shown that biomaterial properties, such as surface topography, stiffness, and chemistry, influence macrophage behavior, with a focus on 2D culture and understanding immune response to materials for implantation or injection.[10,22–26] For example, a range of anti-inflammatory coatings and scaffolds have been designed for applications in tissue regeneration and wound healing. Hydrophilic and rough coatings were observed to promote desired anti-inflammatory and wound healing responses in some cases.[27] Scaffolds made from glycosaminoglycans, such as high molecular weight hyaluronic acid, also have been shown to promote wound healing responses.[28]

Well-defined and tunable 3D culture systems inspired by the native ECM provide an opportunity for better understanding the complex interactions between cells and their microenvironments. Building from the successes of such systems in probing mesenchymal cell-microenvironment interactions,[29–36] we aimed to study immune cell response at homeostasis and in response to pathogens. Studies of macrophages in 3D culture systems for testing hypotheses about how microenvironment cues influence macrophage response to stimuli has gained more recent attention but is less studied, owing in part to the challenges with assaying immune response in 3D cultures.[34,37,38]

Approaches for 3D *in vitro* modeling of the ECM often utilize hydrogels, water-swollen polymer networks, that are engineered to have similar properties to human tissue microenvironments.[30–33] Hydrogels for these applications can be made with building blocks harvested from natural sources, such as collagen, hyaluronic acid, and alginate, or synthesized from synthetic building blocks, such as bioinert polyethylene glycol (PEG) or polyacrylamide and bioactive peptides, with desired functionality.[31,39] While natural polymers have advantages of inherent bioactivity of utility for immune cell culture,[31,39] reductionist approaches with well-defined synthetic building blocks afford the potential for probing the effects of biophysical cues like stiffness independently of specific biochemical cues like receptor-binding sequences. In particular, hydrogels built with bioinert PEG can be attractive for control of synthetic matrix mechanical properties by covalent crosslinking and biochemical content by covalent functionalization with specific bioactive cues for probing cell responses. For example, PEG can be functionalized with a range of biocompatible reactive handles for conjugation with bioactive peptides inspired by natural collagen (*e.g.*, RGD and GFOGER) and cell-degradable linkers that are responsive to matrix metalloproteinases (MMPs) secreted by encapsulated cells, mimicking the dynamics of the ECM.[30,40–42] A few studies have demonstrated the effect of specific extracellular factors on macrophage phenotype and function in 3D culture with engineered ECMs: for example, (i) biochemical content, including identity of the base material (*e.g.*, PEG, gelatin-methacrylate (GELMA), or harvested Collagen I) and presence of individual integrin binding peptides (*e.g.*, RGD, GFOGER, or YISGR), or (ii) biophysical properties, including modulus, pore size, or degradability.[34,38,43,44] These works inspire a reductionist approach to design molecularly engineered culture systems built upon selected polymers and peptides. With harvested ECM hydrogels, decoupling mechanical cues from inherent bioactivity can be challenge. In using a simple, bioinert synthetic building blocks (PEG, peptides), we aim to reproduce only some of the essential elements of *in vivo* systems while providing precise control of microenvironment properties to modulate stiffness independent of selected bioactive cues, complementing natural systems.

The low throughput nature of many manually prepared 3D hydrogel culture systems presents challenges for accessibility across fields and broad use in mechanistic and therapeutic studies that may necessitate hundreds of replicates within a single experiment.[35,39,45,46] Bioprinting has the potential to address these challenges, from the fabrication of polymer scaffolds to single tissues and whole organs. Bioprinting involves automated 3D printing of biocompatible inks, especially those with cells already mixed within the polymeric precursor solution, in a specific spatial organization.[47,48] In particular, drop-on-demand inkjet printing offers the ability to print multiple building blocks into a higher-ordered structure, where the RASTRUM bioprinter creates hydrogel-based structures within a well-plate format for higher throughput of both printing and post-printing cell analysis.[49,50] Bioprinting has gained momentum in the medical field and affords opportunities for creating accessible, robust 3D culture models built with well-defined engineered building blocks, relevant for studying host–pathogen interactions in a range of microenvironments.

In this work, we created a bioinspired controlled 3D culture system for probing macrophage response to bacterial invasion with high throughput using bioprinting[49,51,52] and well-defined synthetic ECMs. Synthetic ECMs were selected to produce stiffnesses like that of healthy to fibrotic lung tissues and present integrin-binding peptides RGD, GFOGER, and YIGSR, relevant to specific ECM proteins (fibronectin, collagens, laminins) found in native human tissues. Human THP-1 monocytes were encapsulated within bioprinted hydrogel-based synthetic ECMs, composed of PEG-peptide building blocks linked with thiol-maleimide chemistry,[49,50,53] and differentiated into macrophages. Macrophage viability,

morphology, phenotype, and inflammatory response to stimuli were assessed within synthetic ECMs with stiffnesses relevant to healthy (storage modulus [G'] ~0.7 and 1.1 kPa) and fibrotic (G' ~3.0 and 4.8 kPa) lung tissues.[30,54] We then applied these high-throughput 3D cultures to study early immune cell response to invasion with pathogenic *Pseudomonas aeruginosa*, a gram-negative bacteria responsible for high mortality rates particularly in patients with cystic fibrosis or other chronic lung disease, developing assays for not only probing immune cell responses but also their uptake of live bacteria.[9,17,55–58] We found differential macrophage responses to *P. aeruginosa* that were dependent on the ECM stiffness, particularly secretion of inflammatory cytokines. These studies establish robust and accessible tools for probing host–pathogen interactions in 3D physiologically relevant microenvironments and demonstrate the importance of ECM stiffness in functional responses of innate immune cells.

Experimental

Cell culture

THP-1 cells (RRID: CVCL_0006), a human monocyte cell line, were purchased from American Type Culture Collection (ATCC, Manassas, Virginia, USA). THP-1 cells were used as a model human macrophage cell line. Cells were confirmed to be contamination free regularly by visual inspection of cell morphologies, sizes, and growth. Cells were also tested on a quarterly basis to be mycoplasma free using MycoAlert® Mycoplasma Detection Kit (Lonza). Cells were cultured between passage 2–10 in complete media, RPMI 1640 Medium (Fisher Scientific) supplemented with 10% heat-inactivated fetal bovine serum (FBS) (certified Gibco heat inactivated, USA origin) and 1% penicillin/streptomycin (Fisher Scientific). THP-1 cells were printed as monocytes, then stimulated with 200 nM phorbol 12-myristate 13-acetate (PMA) (Sigma Aldrich) for 24 hours to differentiate cells into a macrophage phenotype (dTHP-1).[59]

3D Cell encapsulation within hydrogel-based synthetic ECMs

The 3D cultures were printed using the RASTRUM™ bioprinter (Inventia Life Science) based on established protocols.[46,51] Bioinks and activators are proprietary inks sourced from Inventia Life Science (Table 1). These catalog numbers correspond to inks with storage modulus (G') of 0.7, 1.1, 3.0, and 4.8 kPa, where G' is a measure of 'stiffness' (G' ~stiffness k). All inks were generously provided by Inventia Life Science (Sydney, Australia). Inks are composed of a 4-arm PEG-maleimide that reacts with 4-arm PEG-thiol and a combination of thiolated peptides (mono-functionalized integrin binding peptides and di-functionalized MMP-degradable linkers). All inks used in this work included functionalized RGD, GFOGER, and YIGSR. Details of formulations can be found in previous literature.[49,50] The printing protocol was created *via* RASTRUM™ Cloud (Inventia Life Science) using a density of 20E6 cell per mL activator, based on previous work.[51] As a representative example, for one print of 12 wells, you need 200 μL of activator and 20E6 cells per mL in 200 μL of bioink (*i.e.*, activator and bioink are in a 1 : 1 ratio). The activator and bioink come together during inkjet printing in a dropwise fashion for gelation in the well of the well plate.

Table 1 Ink composition for hydrogel matrices

Stiffness (G', kPa)	Activator #	Bioink #	CAS #
0.7	F176	F267	Px01.28
1.1	F177	F239	Px02.28
3.0	F178	F268	Px03.28
4.8	F323	F268	Px06.28

THP-1 monocyte cells were printed using the Large Plug model in a 96-well plate (Corning – #CLS3904). The printed Large Plug model is 0.5 mm in height and fills the whole surface of a well in a standard 96 well plate (surface area ~0.32 cm^2).[60] Post-printing, cells were differentiated with 200 nM PMA for 24 hours. After 24 hours, cells were washed with phosphate buffered saline (PBS) and given fresh complete media. While workflows generally printed monocytes that were then differentiated in 3D culture, differentiated THP-1 macrophages also were printed and yielded similar results (Fig. S1).

Assessment of macrophage viability

The cell viability in 3D culture was assessed by a LIVE/DEAD™ Viability/Cytotoxicity Kit (Invitrogen). The LIVE/DEAD™ kit contained calcein-AM to indicate viable cells (live cells fluoresce green; excitation [ex.] 494 nm, emission [em.] 517 nm) and ethidium homodimer-1 to label dead cells (dead cells fluoresce red; ex. 528 nm, em. 617 nm). Hydrogels were washed 3× with PBS, followed by 3 min PBS incubation, and then incubated (37 °C, 5% CO2) for 10 min in a solution of calcein-AM (2 μM) and ethidium homodimer-1 (4 μM). After incubation, hydrogels were washed 3× with PBS, followed by 3 min PBS incubation. Hydrogels were imaged with a confocal microscope (LSM 800, Zeiss; 10× objective and frame size of 1024 × 1024, 180 μm z-stack, 8.38 μm per slice, three images per sample). Cell viability was quantified with Volocity software (Quorum Technologies Inc.) using the following functions: measure objects and then separate touching objects for AF488 (green) channel and Rhoda (red) channel functions. The percentage of viable cells was calculated by the number of green cells/total number of cells x 100%.

Macrophage polarization

THP-1 cells were printed as monocytes; post-printing, cells were differentiated with 200 nM PMA for 24 hours. After 24 hours, cells were washed with PBS and given fresh complete media. Two days post-printing or seeding, cells were stimulated with either Lipopolysaccharides (LPS) (10 ng mL^{-1}, *Escherichia coli* O111:B4 [Millipore Sigma, Rockville, MD, USA]) and interferon (IFN)-γ (40 ng mL^{-1}, PeproTech®), applied for 72 hours as M1 stimuli.[61,62]

Flow cytometry analysis of macrophage phenotype

All centrifugation steps and washes were completed at 400 g for 5 min within this workflow. Cells on tissue culture polystyrene (TCP) were detached using TrypLE™ Express Enzyme (1×) (Gibco™) for 20 min and washed with PBS. Cells were retrieved from hydrogel matrix to complete downstream flow cytometry analysis. Here, 75 μL (1.1 kPa) or 150 μL (4.8 kPa) of RASTRUM™ Fortissimo Extract (F235, Inventia Life Science) was added to each well for 45 min to enzymatically degrade the hydrogel matrix followed by addition of 100 μL of PBS. Wells were washed 3 times with PBS and subsequent washes were combined and filtered through a 70 μm cell strainer. Cells were washed 2× in 2% FBS in PBS and stained in antibody cocktail for 40 min in the dark on ice. Samples were analyzed using ACEA NovoCyte Flow Cytometer. Antibodies were purchased from Biolegend: Brilliant Violet 711™ anti-human CD86 Antibody (Mouse IgG2b, κ), PE/Cyanine7 anti-human CD206 (MMR) Antibody (Mouse IgG1, κ), Alexa Fluor® 700 anti-human HLA-DR Antibody (Mouse IgG2b, κ), and Pacific Blue™ anti-human CD11b Antibody (Mouse IgG1, κ).

Gene expression of macrophages

Gene expression was measured using Qiagen Custom RT2 Profiler PCR array for genes listed in Table 2 below. Briefly, cells were encapsulated and cultured for 5 days, then retrieved from 3D cultures with F235 (Inventia Life Science), as described above. RNA then was isolated from the retrieved cells using Qiagen RNeasy Micro Kit (cat no. 74004) and subsequently frozen and stored at −80 °C. RNA quality was verified using UV-Vis, where UV A260/A280 ratios all were >2, and Agilent 5200 RNA Fragment Analyzer, where all RNA Quality Numbers (RQNs) were >8. RNA then was converted to cDNA using Qiagen RT First Strand Kit (cat no. 330401) followed by RT2 SYBR Green Fluor qPCR Mastermix Kit (cat no. 330513).

Bacterial cell culture

Two strains of bacteria were used: *P. aeruginosa* (*PAO1*) or *P. aeruginosa*-GFP (10145GFP, ATCC) based on downstream analyses, where GFP-expressing bacteria were used for experiments analyzing macrophage phagocytosis. Bacteria were streaked onto a lysogeny broth (LB) agar plate. Multiple colonies were picked and inoculated into 5 mL of LB for suspension culture. Cells were grown up to exponential phase (OD ~0.6) and then resuspended to an OD of ~2.0 for invasion.

Table 2 Catalog numbers for genes used in custom RT^2 PCR array (Qiagen)

Gene	CAS #
ARG1	PPH20977A
MRC1 (CD206)	PPH09939A
IL10	PPH00572A
IL1B	PPH00171A
TNF	PPH00341A
NFKB1	PPH00204A

Quantification of macrophage phagocytosis of *P. aeruginosa*

THP-1 cells were stained using 1 : 1000 dilution CellTracker™ Deep Red (Invitrogen™) for 30 min in serum free RPMI 1640 media, then washed with RPMI complete media. Cells were allowed to rest for 1 hour before bioprinting. THP-1 cells then were encapsulated in hydrogels, differentiated into macrophages using PMA, and cultured in hydrogels for 4 days in RPMI complete media. On day 4, they were washed 2× (5 min) with antibiotic free RPMI + 10% FBS. Macrophage dTHP-1 cultures were stimulated with 4 μL of *P. aeruginosa*-GFP (diluted to OD = 2) and incubated for 1 hour (37 °C, 5% CO_2), followed by 3× washes in PBS. The 1 hour time point was chosen to have limited bacteria growth within the experimental timeframe, as the bacteria have a doubling time of ~1 hour.[63]

For imaging, dTHP-1s were stained with Hoechst for 25 min then washed 3× prior to invasion. Cells were washed with PBS 3× and fixed in 4% paraformaldehyde (PFA) for 20 minutes. Hydrogels were imaged using the Andor Dragonfly spinning disk confocal (Fusion Software, 25× objective with water immersion and frame size of 2048 × 2048, 4.17 μm slice, 100 μm per stack, three images per sample). Phagocytosis was quantified by IMARIS software using find surfaces. GFP inside macrophages was quantified using a cell mask for cell tracker deep red then finding GFP surfaces within the mask (Fig. S2). For flow cytometry analysis, after 1 hour invasion, dTHP-1 cells were incubated in 1 : 1000 gentamicin: RPMI media for 1 hour, then washed 3× and harvested from the hydrogels as specified in the flow cytometry methods.

Enzyme-linked immunosorbent assay (ELISA) and flow cytometry analysis of *P. aeruginosa* treated macrophages

Four days post-encapsulation, dTHP-1 were washed 2× for 5 min with antibiotic free RPMI + 10% FBS. We then quantified macrophage surface markers and cytokine release after 4-hour invasion and 20-hour rest period. This time period was chosen to allow for sufficient time for cellular responses to bacteria while minimizing any associated cell death, as shown in previous work.[64] Briefly, macrophage dTHP-1 cultures were stimulated with 4 μL of *P. aeruginosa* (POA1) (diluted to OD = 2). After 4 hours of incubation (37 °C, 5% CO_2), cells were treated with 1 : 1000 gentamicin: RPMI media for 1 hour, as previously described,[64] then fresh RPMI media was added. Cells were incubated in media overnight (20 hours). Cells were retrieved from hydrogels and analyzed *via* flow cytometry, following the procedure specified in the flow cytometry methods. Macrophage supernatants were harvested and frozen at −80 °C until shipment for sandwich-based ELISA analysis by University of Maryland Cytokine Core or Human IL1-10 DuoSet ELISA kit (R&D Systems). The limits of quantitation are as follows: IL-1β (0.4 to 2000 pg mL^{-1}), IL-6 (0.18 to 750 pg mL^{-1}), TNF-α (0.4 to 1750 pg mL^{-1}), and IL-10 (31 to 2000 pg mL^{-1}).

Statistical analysis

GraphPad Prism 9 was used to perform statistical analyses. All quantitative data are represented as mean ± standard error of the mean. Tukey's multiple-comparison test was used to generate p-values in one-way ANOVA multiple comparisons unless stated otherwise.

Results and discussion

Bioprinted, bioinspired 3D cultures enable encapsulation and function of differentiated human THP-1 macrophages

To create high-throughput, well-defined 3D cultures for probing host–pathogen interactions, we utilized the RASTRUM™ Bioprinter to encapsulate THP-1 cells in PEG-peptide hydrogel-based synthetic ECMs. These matrices incorporated integrin-binding peptides (YIGSR, GFOGER, RGD) for promoting cell adhesion and function, inspired by native lung ECMs, which are rich in laminins, collagens, and fibronectin amongst other insoluble ECM components. RGD is found in a range of ECM proteins (*e.g.*, fibronectin, collagen I) and was used as a general sequence for promoting binding to a range of integrins (*e.g.*, αvβ3, αvβ5, α5β1);[65] GFOGER is found in collagen I and IV and is known to bind related specific integrins (*e.g.*, α1β1 and α2β1);[66,67] and YIGSR is found in laminins and is known to bind specific integrins (*e.g.*, α1β1 and α3β1).[68] Presence of adhesive sites in the bioprinted PEG network was vital to macrophage viability (Fig. S3). Other compositions were also considered, such as the incorporation of hyaluronic acid (HA), which we previously reported with mouse-derived macrophages[51] and here gave similar viability for bioprinted human THP-1 cells (Fig. S4); however, we chose the reductionist PEG-peptide composition to eliminate concerns over immunomodulatory effects of HA itself.

Hydrogels were fabricated with four different stiffnesses relevant to healthy (G' ~0.7 and 1.1 kPa) and fibrotic (G' ~3.0 and 4.8 kPa) lung tissues. Note, storage moduli (G') reported are estimated to be approximately one-third of the value of the elastic modulus (E) based on rubber elasticity theory (E ~2.1, 3.3, 9.0, 14 kPa, respectively), assuming a Poisson's ratio for an incompressible material (n ~0.5), and are proportional to matrix stiffness.[69] Undifferentiated THP-1 cells were encapsulated in these 3D cultures within a 96-well plate format and then dosed with 200 nM PMA for 24 hours to obtain differentiated macrophages (dTHP-1) (Fig. 1A). These 3D cultures are ~0.5 mm thick and 6.94 mm in diameter with pore sizes that are reported to be similar amongst the different matrix stiffnesses (on the order of ~10 μm^2 based on SEM measurements of the pore area).[49] Hydrogels are rapidly printed (*e.g.*, ~10 minutes to print each plate, not including priming and calibration) for subsequently assaying cell response to different conditions and a range of stimuli with a variety of molecular tools. For imaging applications, production of replicates can be scaled out with the imaging model in which one gel occupies only a fraction of a well, requiring fewer z-stacks. With the imaging models, all 96 wells can be printed in a single run in <2 hours, including preparation and priming of the printer. Through LIVE/DEAD™ staining, we also show that imaging and large plug models created similar cellular microenvironments for 3D culture, with high viability at the same cell densities (Fig. S5). Moving forward, we applied the large plug model to obtain cell counts needed for flow cytometry analyses.

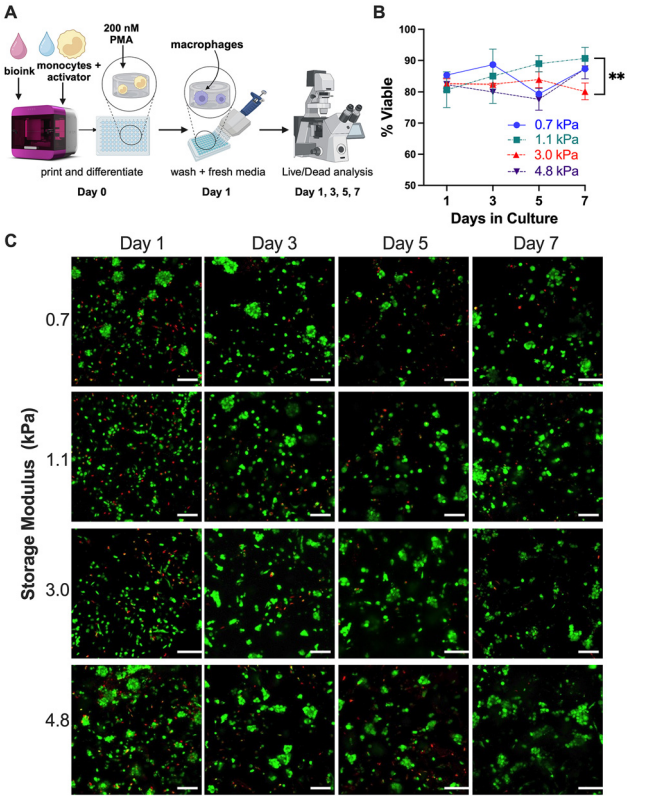

Fig. 1 Cell viability in different matrix compositions in bioprinted 3D cultures. THP-1 monocytes were printed using RASTRUM™ bioprinter and differentiated into macrophages: (A) workflow for cell encapsulation, differentiation, and monitoring. (B) Percentage of viable cells shown with standard error of mean was quantified using analysis of confocal images. The statistics shown represent one-way ANOVA results from Tukey's test ($n \geq 3$), comparing viabilities on Day 7 where *$p < 0.05$, **$p < 0.01$, ***$p < 0.001$, ****$p < 0.0001$. There were statistical differences between Day 7 viability for 1.1 and 3.0 kPa cultures. All others were nonsignificant. (C) Representative z-stack projections from confocal imaging of cells in different synthetic matrix stiffnesses (G' ~0.7, 1.1, 3.0, and 4.8 kPa) stained using LIVE/DEAD™ kit are shown (scale bar: 100 μm).

THP-1 monocytes were encapsulated on Day 0 and differentiated immediately after printing in PMA for 24 hours. Macrophages (dTHP-1) in matrices with different stiffnesses (G' ~0.7, 1.1, 3.0, and 4.8 kPa) all exhibited high viability (>80%) over a 7-day period (Fig. 1B), where Day 1 represents the day following encapsulation and differentiation into dTHP-1s. Viability was confirmed by a secondary measurement of metabolic activity using alamarBlue™ (Fig. S6). The alamarBlue™ results show that metabolic activities of dTHP-1 cells in matrices of different moduli were similar at Day 5, the

timepoint at which the cellular phenotyping and analyses were performed, as detailed below. We downselected to two compositions relevant to healthy and fibrotic lung stiffnesses moving forward.

After confirming viability in all conditions, we chose to focus on 2 matrix compositions inspired by healthy (G' ~1.1 kPa) and fibrotic (G' ~4.8 kPa) lung tissues[30,54] to determine if the mechanical properties of the microenvironment like that found in diseased tissues affected macrophage phenotype and function. Specifically, we wanted to confirm differentiation of monocytes into macrophages using CD11b, which is a surface marker that belongs to the Mac-1 integrin complex and is known to have key functions in macrophage adhesion, migration, phagocytosis, and immune regulation.[70,71] First, macrophages in 3D cultures were differentiated *via* PMA using previously established protocols, and then basal expression of dTHP-1 macrophage surface markers was measured *via* flow cytometry, where representative gating schemes are shown in Fig. S7.[64] An increase in CD11b+ expression (Fig. 2A) compared to the monocyte (no PMA) control indicated successful differentiation of dTHP-1 cells into macrophages, consistent with previous reports.[64,72] Indeed, all THP-1 conditions treated with PMA had >84% CD11b+, a marked increase compared to undifferentiated THP-1 cells on tissue culture polystyrene (THP TCP), which were only ~5% CD11b+. Importantly, we did not see differences in differentiation with PMA when comparing CD11b expression (Fig. 2A) between stiffnesses (1.1 *vs.* 4.8 kPa) or between TCP (positive control) and hydrogel compositions. We did not observe significant proliferation over 7 days (Fig. S6), further supporting that macrophages have been terminally differentiated.

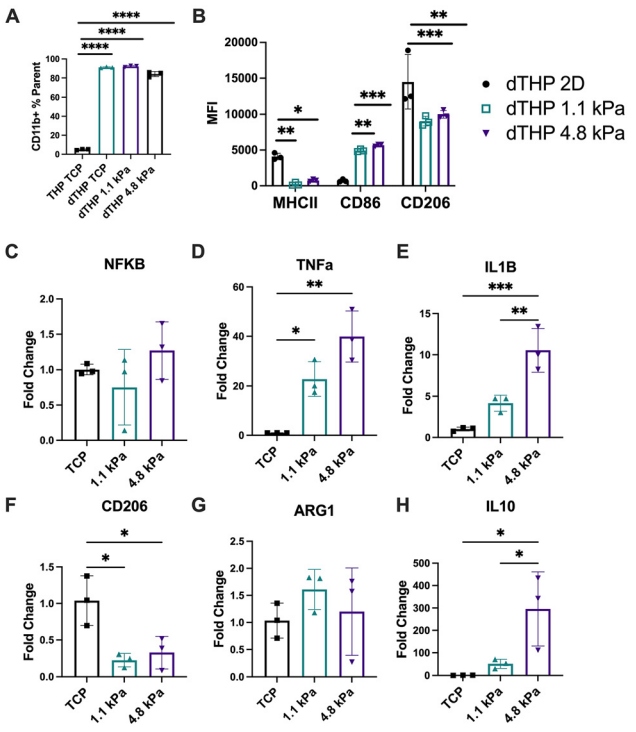

Fig. 2 Basal expression of markers of macrophage phenotype in bioprinted 3D cultures. (A) THP-1 (THP) differentiation into macrophages (dTHP) in different microenvironments (2D culture on TCP; 3D culture in different synthetic matrix stiffnesses (G' ~1.1 kPa, 4.8 kPa)) assessed by the % CD11b + cells using flow cytometry. (B) Basal levels of expression of markers of macrophage phenotype (MHCII, CD86, and CD206) were quantified using flow cytometry. (C–H) Basal levels of expression of markers of macrophage phenotype were quantified using RT-qPCR. The statistics shown represent one-way ANOVA results from Tukey's test (n = 3) where *p < 0.05, **p < 0.01, ***p < 0.001, ****p < 0.0001.

Traditionally, activated macrophages have been characterized with two states—inflammatory phenotypes (M1) or anti-inflammatory phenotypes (M2); however, the spectrum of macrophage phenotype is much broader and more complex than this binary paradigm.[1,10,18,19] Here, expression of CD86 and MHCII (common M1 markers) and CD206 (common M2 marker)[51] for dTHP-1 macrophages was measured after 5 days in 3D culture. There was no statistical difference in surface marker expression (CD86, MHCII, or CD206) between dTHP-1 macrophages cultured in 1.1 and 4.8 kPa synthetic matrices (Fig. 2B); however, there was a significant difference between dTHP-1 macrophages on TCP and dTHP-1 macrophages in 3D cultures. Compared to 2D culture on TCP, dTHP-1 macrophages in 3D cultures had lower CD206 and MHCII and higher CD86 expression. We hypothesize that these 3D cultures provide a more inflammatory microenvironment compared to TCP, which has also been shown in previous literature.[34,37,38] The RT-qPCR data (Fig. 2C–H) confirms the decreased expression of CD206 (Fig. 2F) in 3D culture and also shows increased expression of inflammatory cytokines (TNF-α and IL-1β). In-line with other reports examining matrix density effects, the surface marker data is inconclusive; however, gene expression analysis shows significant differences between soft and stiff matrices.[44] Cells cultured in stiffer (4.8 kPa) synthetic matrix were more activated than cells in more compliant (1.1 kPa) matrices, both in expression of inflammatory (TNF-α and IL-1β) and anti-inflammatory (IL-10) associated genes, supporting the relevance of applying well-defined bioprinted 3D cultures for probing macrophage responses to microenvironment cues.[37]

Macrophage response to well-defined stimuli in bioprinted 3D cultures

For probing macrophage responses in these 3D cultures, well-studied M1 (inflammatory) stimuli (LPS/IFN-γ) were first applied to evaluate M1 polarization. LPS is a stimulus associated with pathogen invasion, where LPS is a found in the outer membrane of gram-negative bacteria and serves as a potent endotoxin that elicits immune responses (Fig. 3).[51,61,62] Importantly, inflammatory stimuli, LPS and IFN-γ, resulted in robust increase expression of MHCII and CD86 in all cultures (2D culture on TCP, 3D cultures with G' ~1.1 kPa, and 4.8 kPa), which are traditionally used as M1 markers.[51,62,73] In response to LPS/IFN-γ, the level of CD86 increase was greater in stiffer matrix while the level of MHC expression was lower in 4.8 compared to 1.1 kPa. Overall, these data indicate appropriate dTHP-1 macrophage polarization in response to stimuli in

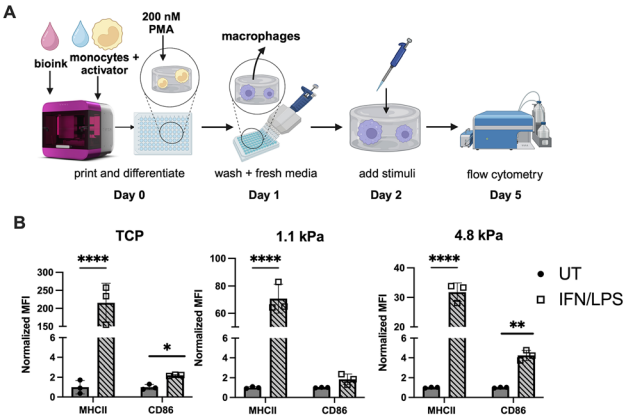

Fig. 3 Macrophage polarization in response to well-defined stimuli in bioprinted 3D cultures. (A) Experimental workflow and (B) flow cytometry results for expression markers of macrophage inflammatory phenotype (MHCII, CD86) in response to well-defined stimuli (M1 stimuli (LPS/IFNγ)) in different microenvironments (2D culture on TCP; 3D culture in different synthetic matrix stiffnesses (G' ~1.1 kPa, 4.8 kPa)). The statistics shown represent a one-way ANOVA Tukey's test (n = 3) where *p < 0.05, **p < 0.01, ***p < 0.001, ****p < 0.0001.

these bioprinted 3D cultures and demonstrate adequate inflammatory response upon application of well-defined stimuli.

Macrophage response to pathogenic bacteria *P. aeruginosa*

After evaluating response to traditional M1 stimuli, we applied our system to study host–pathogen response, by simulating a *Pseudomonas aeruginosa* invasion. *P. aeruginosa* are capable of evading the immune system,[58] often leading to chronic lung infections and overall decreased lung function. Notably, many chronic lung diseases involve constant tissue remodelling, leading to increased stiffness and lung fibrosis.[74,75] Thus, a key question remains: how do such changes in the pulmonary microenvironment, specifically the tissue stiffness, influence macrophage function and their ability to clear pathogens and restore homeostasis? Understanding this relationship is essential for developing new strategies to combat bacterial infections in chronic diseases, but to do so requires new experimental models that accurately capture elements of diseased lung microenvironments to enable mechanistic insights and therapeutic advancements. To probe this, we utilized the bioprinted well-defined 3D cultures evaluate macrophage inflammatory response to invading *P. aeruginosa*, examining phagocytosis of bacteria and cytokine secretion.

Macrophage phagocytosis of these pathogenic bacteria was investigated, invading these 3D cultures with GFP-expressing *P. aeruginosa*. Flow cytometry and image analysis (Fig. 4) confirms phagocytosis of bacteria by a subset of macrophages. As shown in Fig. 4B–F, dTHP-1 macrophages denoted as GFP positive (+) were those that phagocytosed *P. aeruginosa* (Fig. S8). The % of (+) macrophages were similar between 3D cultures (G' ~1.1 and 4.8 kPa) (Fig. 4B). Notably, the (+) macrophages harvested from 1.1 kPa hydrogels exhibited a higher

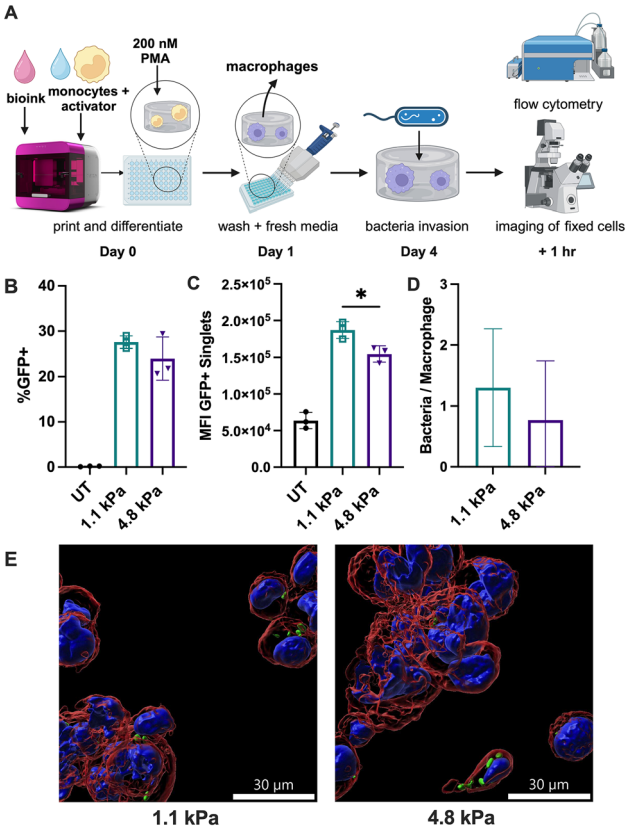

Fig. 4 Analysis of GFP-expressing *P. aeruginosa* uptake by macrophages. (A) Workflow of bacteria invasion. Flow cytometry results showing (B) % of dTHP-1 macrophages that are GFP+; and (C) GFP MFI of only macrophages that are + for bacteria phagocytosis, for cells in 2D culture on TCP without bacterial invasion (UT control) and 3D culture in different synthetic matrix stiffnesses with bacterial invasion (G' ~1.1 kPa, 4.8 kPa). (D) average bacteria/cell/image was quantified using IMARIS analysis of (E) confocal microscopy images to identify GFP + bacteria (green) within macrophage cell bodies stained with CellTracker™ (red) and nuclei (blue). Image processing can be found in Fig. S2. The statistics shown represent one-way ANOVA (B–D) Tukey's test (n = 3) where *p < 0.05, **p < 0.01, ***p < 0.001, ****p < 0.0001.

GFP MFI than those from 4.8 kPa (Fig. 4C). The complementary image analysis (Fig. 4D) confirms internalization of bacteria, where bacteria invasion through the full thickness of the synthetic matrix was observed in both conditions. Movement of bacteria was enabled in part by the average estimated pore size of these bioprinted 3D cultures (~10 microns) being larger than individual bacteria (diameter ~1 micron). The number of bacteria per dTHP-1 macrophage suggests that the macrophages have similar levels of phagocytosis in 1.1 and 4.8 kPa matrices; however, the mean phagocytosis and associated distribution trend is higher in the 1.1 kPa condition (Fig. 4D), consistent with the flow cytometry data. These observations suggest that, within the population of macrophages that internalized bacteria, macrophages in 1.1 kPa condition phagocytosed more bacteria per cell than those in 4.8 kPa condition; however, overall, macrophages in both matrices exhibit similar phagocytosis levels.

We further probed host–pathogen interactions in these microenvironments by investigating dTHP-1 macrophage phenotypic and inflammatory responses to bacteria through flow cytometry and ELISA, quantifying inflammatory surface markers and cytokine secretion, respectively. Macrophages exhibited increases in both inflammatory surface markers, CD86 and MHCII, in response to *P. aeruginosa* after 4-hour invasion with bacteria (Fig. 5 and Fig. S9).

The expression levels of surface markers were similar in both 3D culture conditions invaded with *P. aeruginosa* (1.1 kPa and 4.8 kPa) (Fig. 5). MHCII expression was higher and CD86 expression was lower in the 1.1 kPa condition compared to 4.8 kPa condition. To our knowledge, this report is the first flow cytometry phenotypical analysis of human macrophage response to *P. aeruginosa* in an *in vitro* 3D microenvironment. In both conditions, an increase in inflammatory cytokines (TNF-α, IL-1β, IL-6) was observed upon invasion using ELISA, consistent with other *in vitro* bacteria invasion assays.[7,8] Along with inflammatory cytokines, we observed an increase in an anti-inflammatory cytokine IL-10. These observations of increases in both anti-inflammatory and inflammatory cytokine production in response to *P. aeruginosa* has been reported in the literature.[8,76] A statistically significant increase in IL-10 also was observed in the fibrotic matrix condition compared to its UT condition; this increase is consistent with literature showing that stiffness can increase alternatively activated (M2) macrophages.[30,77]

We observed statistical differences in the levels of secreted cytokines between cultures as well, where cells in 3D cultures inspired by fibrotic microenvironments (G' ~4.8 kPa) secreted lower amounts of IL-6 and IL-1β, and higher amounts of TNF-α and IL-10 compared to cells in more compliant matrices inspired by healthy microenvironments. These observations of varying levels of response between fibrotic *versus* healthy microenvironments suggests potential origins of chronic immune evasion and supporting culture model relevance as discussed below. Overall, these studies provide critical workflows for immune cell phenotypical analysis in 3D cultures of host–pathogen cells and insights into macrophage responses to pathogenic bacteria in 3D microenvironments inspired by healthy and fibrotic lung tissue.

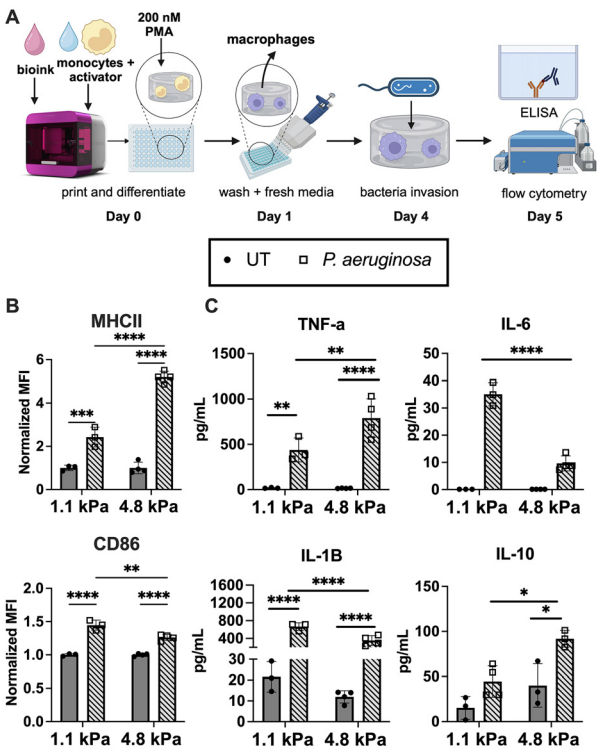

Fig. 5 Evaluation of macrophage inflammatory response to *P. aeruginosa*. (A) Workflow is shown for (B) flow cytometry result for macrophage surface markers and (C) ELISA results of measured cytokine release for macrophages in 3D culture in synthetic matrix stiffnesses (G' ~1.1 kPa, 4.8 kPa) with and without (UT) *P. aeruginosa* invasion. The statistics shown represent one-way ANOVA Tukey's test (n = 3) where *p < 0.05, **p < 0.01, ***p < 0.001, ****p < 0.0001.

Discussion

The role of the microenvironment in cellular phenotypes and functions, including for immune cells like macrophages, is becoming increasingly implicated in the context of chronic diseases. This underscores the need for accessible and consistent 3D culture systems to study cellular responses to chemical and mechanical cues presented by the ECM and to other cells found within a range of niches.[78,79] Within hydrogel-based 3D cultures, many factors have been identified to influence macrophage phenotype and function, including the chemical composition, integrin binding peptides, modulus, pore size, and degradability of the matrix.[34,38,43] Further, macrophages recently were found to use a fundamentally different mechanism for mechanosensing of their environment when encapsulated within *versus* seeded on top of substrates, highlighting the importance of recapitulating physiologically relevant microenvironments *in vitro*.[79] Given that chronic lung diseases are characterized by extensive ECM remodelling and fibrosis, leading to altered macrophage function and impaired immune responses, model systems that capture these microenvironmental changes with high throughput are essential for probing the mechanisms of immune dysfunction and identifying potential therapeutic targets.

In this work, we utilized synthetic ECMs formed from thiol–ene chemistry using building blocks of bioinert PEGs functionalized with maleimide or thiol groups and thiolated peptides. Thiol-maleimide hydrogels are well-characterized and known to be highly stable for >30 days in the absence of MMP-degradation.[80] In our hands, the thickness of the gel remained constant over the course of the study, based on confocal imaging; therefore, we did not see evidence of degradation of gels over a 7-day period. For longer periods of time, future work could measure cell-driven degradation, which is dependent on cell type, density, and stimuli. Further this chemistry has been demonstrated previously to produce high viability of encapsulated cells, without the need for light-based

or small molecule initiators,[81–83] and shown relevance for a range of biological applications (*e.g.*, cell culture, tissue engineering, drug delivery).[81,82,84] While the fast reaction kinetics can present challenges in manually prepared materials,[81–83] inkjet-based bioprinting takes advantage of this rapid gelation to form well-defined 3D cultures within a well-plate format using a controlled, drop-wise approach.[49,50] Our group[51] and others[46,49,53] have previously shown that this inkjet printing efficiently encapsulates a variety of cell types, including cancer cells, fibroblasts, and murine primary and immortalized macrophages.[51] Here, we build upon that work and show that this bioprinting technology can be used to create high-throughput, well-defined, and adaptable synthetic 3D cultures of human macrophages and probe their responses to inflammatory factors and a bacterial pathogen.[46,85,86]

The presented work uniquely demonstrates how inkjet-based bioprinting can be utilized for encapsulation and culture of human macrophages for high-throughput probing of host–pathogen interactions. To achieve this, we developed consistent workflows for encapsulating, differentiating, and analysing THP-1 human macrophages. While we focused on encapsulation of THP-1 monocytes followed by their differentiation to macrophages in 3D culture, we have also demonstrated that fully differentiated THP-1 macrophages can be printed, encapsulated, and cultured (Fig. S1). As prior work has shown photopolymerized PEG-peptide hydrogels did not allow for viable encapsulation of human dTHP-1 macrophages,[64] our contrasting results further support the versatility of the bioprinted thiol-maleimide PEG-peptide hydrogel 3D culture platform for studies of innate immune cells. We utilized the range of capabilities provided by bioprinting to probe cell responses to different matrix stiffnesses, as well as hydrogel model architectures, and developed a range of workflows for key assays and cell analyses to probe macrophage phenotypic, phagocytic, and inflammatory responses to stimuli in these bioinspired 3D microenvironments. Over a range of stiffness relevant to healthy and fibrotic tissues, we translated protocols from traditional TCP to multi-well plate 3D cultures for simple and accessible workflows that allow cell harvesting for flow cytometry or high-resolution *in situ* imaging. In these 3D cultures, regardless of stiffness, macrophages remained viable and responsive to external stimuli and produced relevant inflammatory responses (Fig. 3).

We focused on evaluating the effect of stiffness on macrophage response to bacterial invasion in these 3D cultures. First, we evaluated successful differentiation from monocytes to macrophages indicated by CD11b+ expression (Fig. 2A) and appropriate macrophage M1 polarization (Fig. 3B). Then, upon adding *P. aeruginosa*, we observed that human macrophages produce phenotypic and cytokine profiles consistent with those observed during pathogen invasion *in vivo*,[9,87] mainly upregulation of inflammatory markers (MHCII and CD86) and inflammatory protein secretion (IL-1β, TNF-α, and IL-6) (Fig. 5). Toll-like receptor (TLR) ligands on the bacteria cell wall, mainly LPS and flagella, are known to upregulate both MHCII and CD86,[88,89] which is confirmed by this work. These two surface markers also are important for antigen presentation to T-cells. When macrophages engulf bacteria small peptide fragments are processed in the endosome and then displayed and presented by MHC for presentation to T-cells, and CD86 acts as a costimulatory molecule for promoting T-cell activation and proliferation.[90] Aside from T-cell stimulation, macrophages also fight off bacterial infection through release of reactive oxygen species (ROS) and nitric oxide (NO),[91] as well as many inflammatory cytokines including those tested in this study (IL-1β, TNF-α, and IL-6).[1–13] These cytokines are all essential in the host immune response and accordingly are among the most commonly studied in previous invasion models.[8,16,64,89,92,93] The inflammatory and antimicrobial response of macrophages to *P. aeruginosa* in 3D culture platform is consistent with literature reports, including macrophage responses on TCP to invasion with *P. aeruginosa*,[8,64,91] and now provides insights into responses in well-defined 3D microenvironments with different physiologically-relevant stiffnesses.

Notably, when the stiffness of microenvironment was varied from a healthy (1.1 kPa) to fibrotic range (4.8 kPa), RT-qPCR analysis showed changes in the expression of several genes, where macrophages in the 4.8 kPa condition expressed higher levels of both inflammatory and anti-inflammatory genes compared to 1.1 kPa. This observation is consistent with constant, aberrant wound healing, where macrophages are persistently activated in the fibrotic niche and other chronic lung diseases.[94,95]

We did not observe differences in basal levels of expression of inflammatory surface markers or protein secretion between fibrotic and healthy ECM-mimics, whereas we did observe statistical differences in macrophage phagocytosis, protein secretion, and surface marker expression in response to bacterial invasion between 3D cultures of different compliance (Fig. 4 and 5). While the percentage of macrophages that phagocytosed bacteria was similar between conditions, higher amounts of bacteria per macrophage were discerned in the healthy lung microenvironment condition (1.1 kPa) compared to the fibrotic lung microenvironment condition (4.8 kPa). These findings from flow cytometry analysis, supported by super-resolution imaging trends, suggest increased macrophage phagocytic activity in the healthy microenvironment; however, only small differences are seen. More complex culture systems, such as co-culture with other host cells (*e.g.*, epithelial cells, fibroblasts), may elucidate more pronounced differences. Further, macrophage secretion of IL-1β and IL-6 during infection was higher within the healthy microenvironment, whereas TNF-α and IL-10 secretion was higher in the fibrotic microenvironment.

Each of these cytokines has essential functions. IL-1β release is indicative of inflammasome activation, which is essential in controlling bacterial growth and balancing the duration and strength of macrophage inflammatory responses.[96] Previous studies by Deng *et al.* in TCP also show that *P. aeruginosa* activates the NLRP3 inflammasome, marked

by release of IL-1β.[7] IL-6 is often associated with acute reactions to infections and plays critical roles in recruiting leukocytes to the infection site, while also promoting anti-inflammatory resolution.[92,97] TNF-α plays an essential role in fighting off bacterial infections, through a broad range of functions, such as recruitment of neutrophils, signalling cell death, and stimulation of adjacent cells to secrete antimicrobial peptides.[98] Note, amongst these cytokines, TNF-α is known to have multi-functional pro-immune activities that are context dependent. The level of TNF-α is important for promoting beneficial, pro-healing responses to injury and invaders, including an effective host response to pathogen invasion; however, excessive activation of TNF-α-mediated cell death is known to promote, rather than prevent, microorganism pathogenicity.[99–101]

Unlike the other cytokines measured, IL-10 is known to be immunosuppressive and is characteristic of anti-inflammatory M2 macrophages.[102,103] Because macrophages are highly plastic, heterogeneous, and exist along a spectrum of M1 to M2 phenotypes, macrophages can upregulate both inflammatory and anti-inflammatory factors simultaneously.[8,104] M2 macrophages may be responsible for promoting fibrosis; however, the role of IL-10 in pulmonary fibrosis remains unclear. While IL-10 is an essential regulator to balance inflammation and prevents excessive tissue damage,[105,106] IL-10 can be a driver of pulmonary fibrosis[107] and a tolerizing factor that may explain decreased bacteria clearance in fibrotic microenvironments. Whether IL-10 promotes or resolves bacterial infection also remains debated.

On the whole, upregulation of all these proteins show that macrophages exhibit a robust response to *P. aeruginosa* in both the healthy and fibrotic inspired compositions (1.1 and 4.8 kPa) of these bioprinted 3D cultures. However, in the fibrotic microenvironment, we see downregulation of proteins that are essential for resolving infection, IL-6 and IL-1β, and upregulation of TNF-α, which can cause negative immune impacts if overexpressed. Further, increases in IL-10 are consistent with macrophages in fibrotic environments, where M2 activation is prominent.[108,109] Additionally, basal gene expression levels of macrophages are consistent with a continual overactivated state, which is often seen in chronic lung disease and fibrosis. Taken together, gene expression and protein secretion data show the complexity of macrophage polarization, where macrophages are not solely M1 or M2 but can upregulate traditional M1 and M2 markers simultaneously; it is now widely accepted that macrophages exist on a spectrum rather than a binary scale.[95,110] These studies suggest the relevance of the high-throughput 3D culture system for probing dysregulated or suppressed macrophage response in lung disease.

This work establishes a high-throughput 3D culture platform as a powerful tool for studying immune responses in chronic lung infections, demonstrating that ECM stiffening may play a vital role in the macrophage-mediated pathogen clearance and inflammatory response. While our study focuses on acute immune responses due to the inherent limitations of *in vitro* co-cultures, where long bacterial invasion times (>24 hours, Fig. S9) are often impractical,[8,64,93,111,112] this system provides a foundation for investigating microenvironmental influences on infection initiation. Beyond stiffness, this platform can be adapted to evaluate different microenvironment cues, such as viscoelasticity, collagen and other protein deposition, and multicellular interactions. Further, while our studies have focused on macrophage response, these culture systems may also be relevant for studying bacteria response to related microenvironment cues, where mechanical properties also have been shown to influence bacteria function.[113–115] Along with macrophages, the interplay between immune cells and other cells found in the lung microenvironment, such as fibroblasts, plays an important role in fibrosis and response to microenvironment stimuli (*e.g.*, mechanical stiffness, pathogens). Opportunities for future work include increasing model system complexity for evaluation of immune responses to pathogens with both macrophages and fibroblasts in these bioprinted 3D cultures. Further, while cell lines are relevant for preliminary testing of technology and allow the robust screening of immune responses, evaluating the responses of primary immune cells with the approaches established here will be relevant in future studies particularly for use of cells from different origins (*e.g.*, healthy *vs.* diseased individuals). Additionally, while we focused on probing response of macrophages to the microenvironment, there are opportunities to use this system to also evaluate monocyte response to microenvironment cues prior to differentiation.

Overall, this work establishes a foundation for using this high throughput bioprinting platform for answering important mechanistic questions. By varying synthetic matrix biochemical content, stiffness, model architecture, this system enables precise control over environmental variables, facilitating investigations into cellular responses to pathogens, cytokines, and therapeutic interventions. With its potential for both fundamental research and high-throughput drug screening, this technology provides a valuable framework for identifying strategies to enhance immune function and pathogen clearance in fibrotic lung diseases.

Conclusions

We demonstrated a high-throughput, tunable, versatile 3D culture system for probing host–pathogen interactions, specifically macrophage responses to microenvironment cues and bacterial invasion. Workflows were established that allow interrogation of macrophage responses in these 3D cultures, including polarization, cytokine secretion, and phagocytosis, and enabled new studies to build from those previously done in 2D culture or manually prepared 3D cultures. We show that the bioprinting process for creating these 3D cultures is compatible with human innate immune cells, allowing high viability of THP-1 monocytes and dTHP-1 macrophages in synthetic ECMs of varying compliance over a range relevant for healthy to fibrotic lung tissue. With this model system, we found

differential immune response in stiffer, fibrotic microenvironments compared to more compliant, healthy microenvironments. This altered immune response suggests potential origins of chronic immune evasion observed clinically. Overall, this work established a platform for modeling and understanding immune response in bioinspired tissue microenvironments, providing well-defined, yet more complex co-cultures with insights into macrophage responses to different stimuli and future opportunities for use in mechanistic and treatment studies.

Author contributions

J. G.: conceptualization, data curation, formal analysis, investigation, visualization, writing – original draft preparation; D. M.: conceptualization, visualization, formal analysis; C. G.: project administration, funding acquisition; C. F.: funding acquisition, supervision, writing – review & editing; A. K.: project administration, funding acquisition, supervision, writing – review & editing.

Conflicts of interest

There are no conflicts to declare.

Data availability

All data available upon request to corresponding author. Supplementary information (SI) is available. See DOI: https://doi.org/10.1039/d5lp00285k.

Acknowledgements

This work was supported by grants for related work from a National Institutes of Health (NIH) Director's New Innovator Award with grant number DP2HL152424 (Kloxin), a NIH National Institute of General Medicine (NIGMS) Award with grant number R35GM142866A (Fromen), Delaware Bioscience Center for Advanced Technology grant (12A00448), and Defense Threat Reduction Agency (DTRA) CBM (HDTRA1448297). Additionally, the authors acknowledge the use of facilities and instrumentation supported by the National Science Foundation (NSF) through the University of Delaware Materials Research Science and Engineering Center (DMR-2011824) and the NIH National Institute of General Medical Sciences (NIGMS) through the Delaware COBRE (P20GM104316). Access to microscopy and analysis software within Delaware Biotechnology Institute (DBI) BioImaging was supported by the Institutional Development Award (IDeA) from the NIH NIGMS under grant number P20GM103446, as well as NIGMS (P20 GM139760) and the State of Delaware. The authors thank the DBI Bioimaging Core, specifically Jeffrey Caplan and Chandran Sabanayagam, for training and assistance in imaging and image analysis of bacterial phagocytosis and DBI DNA Sequencing Core and Genotyping Core, specifically Brewster Kingham and Mark Shaw. The authors thank Claire Lois for support of bacteria cultures and Inventia Life Science for use and support of the RASTRUM™ bioprinter, especially Dwayne Dexter and Whitney Symons. Additional student support was obtained from the Collins fellowship and NSF Graduate Research Fellowship Program (GRFP) Award number 1940700 (Graf) and NIH Chemistry-Biology Interface program supported by the NIGMS of the NIH (T32GM133395) (Moore). The content is solely the responsibility of the authors and does not necessarily represent the official views of the NIH, NSF, or DTRA CBM. Fig. 1A, 3A, 4A, and 5A were created using BioRender.com.

References

1 H. Aegerter, B. N. Lambrecht and C. V. Jakubzick, *Immunity*, 2022, **55**, 1564–1580.
2 M. B. Buechler, W. Fu and S. J. Turley, *Immunity*, 2021, **54**, 903–915.
3 M. d. W. Amy, S. H. Pieter, H. M. O. Tom, A. J. Simone and M. v. d. D. Anne, *Thorax*, 2022, **77**, 408.
4 D. Hirayama, T. Iida and H. Nakase, *Int. J. Mol. Sci.*, 2017, **19**, 92.
5 A. Ardain, M. J. Marakalala and A. Leslie, *Immunology*, 2020, **159**, 245–256.
6 M. Ciszek-Lenda, M. Strus, M. Walczewska, G. Majka, A. Machul-Żwirbla, D. Mikołajczyk, S. Górska, A. Gamian, B. Chain and J. Marcinkiewicz, *Inflammation Res.*, 2019, **68**, 397–413.
7 Q. Deng, Y. Wang, Y. Zhang, M. Li, D. Li, X. Huang, Y. Wu, J. Pu and M. Wu, *Infect. Immun.*, 2016, **84**, 56–66.
8 A. V. Jäger, P. Arias, M. V. Tribulatti, M. A. Brocco, M. V. Pepe and A. Kierbel, *Sci. Rep.*, 2021, **11**, 2393.
9 E. G. Lavoie, T. Wangdi and B. I. Kazmierczak, *Microbes Infect.*, 2011, **13**, 1133–1145.
10 T. Tylek, J. Wong, A. E. Vaughan and K. L. Spiller, *Biomaterials*, 2024, **308**, 122545.
11 E. Seydoux, K. Fytianos, C. v. Garnier, B. Rothen-Rutishauser and F. Blank, *J. Aerosol Med. Pulm. Drug Delivery*, 2024, **37**, 328–337.
12 E.-K. Jo, *Exp. Mol. Med.*, 2019, **51**, 1–3.
13 K. A. Wodzanowski, S. E. Cassel, C. L. Grimes and A. M. Kloxin, *Bioorg. Med. Chem. Lett.*, 2020, **30**, 127116.
14 A. Agrawal, *Int. J. Mol. Sci.*, 2017, **18**, DOI: 10.3390/ijms18061206.
15 R. Rosales-Reyes, P. Garza-Villafuerte, D. Vences-Vences, D. F. Aubert, R. Aca-Teutle, V. F. Ortiz-Navarrete, L. C. Bonifaz, J. C. Carrero-Sánchez, A. Olivos-García, M. A. Valvano and J. I. Santos-Preciado, *Emerging Microbes Infect.*, 2020, **9**, 2000–2012.
16 E. Kaya, L. Grassi, A. Benedetti, G. Maisetta, C. Pileggi, M. Di Luca, G. Batoni and S. Esin, *Front. Cell. Infect. Microbiol.*, 2020, **10**, 187.

17 W. J. Rowe, D. A. Lebman and D. E. Ohman, *Front. Cell. Infect. Microbiol.*, 2023, **13**, 1125901.
18 G. Sreejit, A. J. Fleetwood, A. J. Murphy and P. R. Nagareddy, *Clin. Transl. Immunol.*, 2020, **9**, e1222.
19 J. Graf, M. Trautmann-Rodriguez, S. Sabnis, A. M. Kloxin and C. A. Fromen, *Eur. J. Pharm. Sci.*, 2023, **191**, 106596.
20 R. Annoni, T. Lanças, R. Y. Tanigawa, M. d. M. Matsushita, S. d. M. Fernezlian, A. Bruno, L. F. F. d. Silva, P. J. Roughley, S. Battaglia, M. Dolhnikoff, P. S. Hiemstra, P. J. Sterk, K. F. Rabe and T. Mauad, *Eur. Respir. J.*, 2012, **40**, 1362–1373.
21 T. Bhattacharya, A. Bej, A. Das, S. S. Bartwal and A. Nandi, *Regener. Eng. Transl. Med.*, 2025, DOI: 10.1007/s40883-025-00499-6.
22 S. D. Dutta, K. Ganguly, T. V. Patil, A. Randhawa and K. T. Lim, *Bioact. Mater.*, 2023, **28**, 284–310.
23 A. J. Clevenger, A. Jha, E. Moore and S. A. Raghavan, *Trends Biotechnol. (Regular ed.)*, 2025, **43**, 131–144.
24 L. Morales-Nebreda, A. V. Misharin, H. Perlman and G. R. S. Budinger, *Eur. Respir. Rev.*, 2015, **24**, 505–509.
25 D. M. Mosser and J. P. Edwards, *Nat. Rev. Immunol.*, 2008, **8**, 958–969.
26 A. Shapouri-Moghaddam, S. Mohammadian, H. Vazini, M. Taghadosi, S. A. Esmaeili, F. Mardani, B. Seifi, A. Mohammadi, J. T. Afshari and A. Sahebkar, *J. Cell Physiol.*, 2018, **233**, 6425–6440.
27 J. Mao, L. Chen, Z. Cai, S. Qian, Z. Liu, B. Zhao, Y. Zhang, X. Sun and W. Cui, *Adv. Funct. Mater.*, 2022, **32**, 2111003.
28 S. Hauck, P. Zager, N. Halfter, E. Wandel, M. Torregrossa, A. Kakpenova, S. Rother, M. Ordieres, S. Räthel, A. Berg, S. Möller, M. Schnabelrauch, J. C. Simon, V. Hintze and S. Franz, *Bioact. Mater.*, 2021, **6**, 4342–4359.
29 S. Schlie-Wolter, A. Ngezahayo and B. N. Chichkov, *Exp. Cell Res.*, 2013, **319**, 1553–1561.
30 K. Bomb, L. Pradhan, Q. Zhang, B. M. Jarai, A. Bhattacharjee, D. L. Burris, A. M. Kloxin and C. A. Fromen, *Biomater. Sci.*, 2022, **10**, 5689–5706.
31 S. R. Caliari and J. A. Burdick, *Nat. Methods*, 2016, **13**, 405–414.
32 J. Lou and D. J. Mooney, *Nat. Rev. Chem.*, 2022, **6**, 726–744.
33 M. Sreepadmanabh, A. B. Arun and T. Bhattacharjee, *Biophys. Rev.*, 2024, **5**, 021304.
34 B. H. Cha, S. R. Shin, J. Leijten, Y. C. Li, S. Singh, J. C. Liu, N. Annabi, R. Abdi, M. R. Dokmeci and N. E. Vrana, *Adv. Healthcare Mater.*, 2017, **6**, 1700289.
35 N. Chaicharoenaudomrung, P. Kunhorm and P. Noisa, *World J. Stem Cells*, 2019, **11**, 1065–1083.
36 T. E. Sutherland, D. P. Dyer and J. E. Allen, *Science*, 2023, **379**, eabp8964.
37 M. Kim, S. Lee and C. S. Ki, *ACS Biomater. Sci. Eng.*, 2019, **5**, 922–932.
38 S. Lee and C. S. Ki, *Carbohydr. Polym.*, 2020, **229**, 115555.
39 W. Fang, M. Yang, L. Wang, W. Li, M. Liu, Y. Jin, Y. Wang, R. Yang, Y. Wang, K. Zhang and Q. Fu, *Int. J. Bioprint.*, 2023, **9**, 759.
40 E. M. Ford, A. M. Hilderbrand and A. M. Kloxin, *J. Mater. Chem. B*, 2024, **12**, 9600–9621.
41 M. E. Smithmyer, S. E. Cassel and A. M. Kloxin, *AIChE J.*, 2019, **65**, e16837.
42 K. L. Wiley, B. P. Sutherland, B. A. Ogunnaike and A. M. Kloxin, *Adv. Healthc. Mater.*, 2022, **11**, e2101947.
43 M. Cicuéndez, A. García-Lizarribar, L. Casarrubios, M. J. Feito, F. J. Fernández-San-Argimiro, N. García-Urkia, O. Murua, I. Madarieta, B. Olalde, R. Diez-Orejas and M. T. Portolés, *Biomater. Adv.*, 2024, **159**, 213794, DOI: 10.1016/j.bioadv.2024.213794.
44 J. Sapudom, W. K. E. Mohamed, A. Garcia-Sabaté, A. Alatoom, S. Karaman, N. Mahtani and J. C. Teo, *Bioengineering*, 2020, **7**, 7020033.
45 S. D. Dutta, T. V. Patil, K. Ganguly, A. Randhawa and K.-T. Lim, *Bioact. Mater.*, 2023, **28**, 284–310.
46 M. Engel, L. Belfiore, B. Aghaei and M. Sutija, *SLAS Technol.*, 2022, **27**, 32–38.
47 A. t. Sachdev, S. Acharya, T. Gadodia, S. Shukla, J. Harshita, C. Akre, M. Khare and S. Huse, *Cureus*, 2022, **14**, e28463.
48 B. Yilmaz, A. Al Rashid, Y. A. Mou, Z. Evis and M. Koç, *Bioprinting*, 2021, **23**, e00148.
49 E. Y. Du, M. Jung, J. Skhinas, M. A. K. Tolentino, J. Noy, N. Jamshidi, J. L. Houng, K. C. Tjandra, M. Engel, R. Utama, R. D. Tilley, M. Kavallaris and J. J. Gooding, *ACS Appl. Bio Mater.*, 2023, **6**, 4603–4612.
50 R. H. Utama, V. T. G. Tan, K. C. Tjandra, A. Sexton, D. H. T. Nguyen, A. P. O'Mahony, E. Y. Du, P. Tian, J. C. C. Ribeiro, M. Kavallaris and J. J. Gooding, *Macromol. Biosci.*, 2021, **21**, 2100125.
51 J. Graf, K. Bomb, M. Trautmann-Rodriguez, B. M. Jarai, N. Gill, A. M. Kloxin and C. A. Fromen, *Front. Biomater. Sci.*, 2024, **3**, 1399448.
52 M. A. Sullivan, S. Lane, A. Volkerling, M. Engel, E. L. Werry and M. Kassiou, *Biotechnol. Bioeng.*, 2023, **120**, 3079–3091.
53 M. Jung, J. N. Skhinas, E. Y. Du, M. A. K. Tolentino, R. H. Utama, M. Engel, A. Volkerling, A. Sexton, A. P. O'Mahony, J. C. C. Ribeiro, J. J. Gooding and M. Kavallaris, *Biomater. Sci.*, 2022, **10**, 5876–5887.
54 T. Guo, C. He, A. Venado and Y. Zhou, *Compr. Physiol.*, 2022, **12**, 3523–3558.
55 I. Jurado-Martín, M. Sainz-Mejías and S. McClean, *Int. J. Mol. Sci.*, 2021, **22**, 22063128.
56 M. Ciszek-Lenda, G. Majka, M. Suski, M. Walczewska, S. Górska, E. Golińska, A. Fedor, A. Gamian, R. Olszanecki, M. Strus and J. Marcinkiewicz, *Inflammation Res.*, 2023, **72**, 1275–1289.
57 G. John, A. O. Yildirim, B. K. Rubin, D. C. Gruenert and M. O. Henke, *Am. J. Respir. Cell Mol. Biol.*, 2010, **42**, 424–431.
58 A. M. Sousa and M. O. Pereira, *Pathogens*, 2014, **3**, 680–703.
59 T. Kochiyama, X. Li, H. Nakayama, M. Kage, Y. Yamane, K. Takamori, K. Iwabuchi and E. Inada, *Mediators Inflammation*, 2019, **2019**, 1919538.
60 N. Gomila Pelegri, A. M. Stanczak, A. L. Bottomley, B. K. Milthorpe, C. A. Gorrie, M. P. Padula and J. Santos, *Int. J. Mol. Sci.*, 2023, **24**, 12139.

61 E. W. Baxter, A. E. Graham, N. A. Re, I. M. Carr, J. I. Robinson, S. L. Mackie and A. W. Morgan, *J. Immunol. Methods*, 2020, **478**, 112721.
62 M. Genin, F. Clement, A. Fattaccioli, M. Raes and C. Michiels, *BMC Cancer*, 2015, **15**, 577.
63 A. E. LaBauve and M. J. Wargo, *Curr. Protoc. Microbiol.*, 2012, 6E.1.1–6E.1.8.
64 K. A. Wodzanowski, J. L. Caplan, A. M. Kloxin and C. L. Grimes, *Front. Chem.*, 2022, **10**, 842602.
65 B. S. Ludwig, H. Kessler, S. Kossatz and U. Reuning, *Cancers*, 2021, **13**, 13071711.
66 Q. Zhang, S. Zhang, J. Chen and Z. Xie, *Int. J. Mol. Sci.*, 2023, **24**, 24076170.
67 M. E. Smithmyer, J. B. Spohn and A. M. Kloxin, *ACS Biomater. Sci. Eng.*, 2018, **4**, 3304–3316.
68 J. E. Frith, R. J. Mills, J. E. Hudson and J. J. Cooper-White, *Stem Cells Dev.*, 2012, **21**, 2442–2456.
69 M. S. Rehmann, J. I. Luna, E. Maverakis and A. M. Kloxin, *J. Biomed. Mater. Res., Part A*, 2016, **104**, 1162–1174.
70 H. Atcha, V. S. Meli, C. T. Davis, K. T. Brumm, S. Anis, J. Chin, K. Jiang, M. M. Pathak and W. F. Liu, *Front. Immunol.*, 2021, **12**, 689397.
71 M. A. Arnaout, *Blood*, 1990, **75**, 1037–1050.
72 T. Starr, T. J. Bauler, P. Malik-Kale and O. Steele-Mortimer, *PLoS One*, 2018, **13**, e0193601.
73 T. D. Smith, M. J. Tse, E. L. Read and W. F. Liu, *Integr. Biol.*, 2016, **8**, 946–955.
74 H. I. Warheit-Niemi, S. J. Edwards, S. SenGupta, C. A. Parent, X. Zhou, D. N. O'Dwyer and B. B. Moore, *JCI Insight*, 2022, **7**, e152690.
75 M. Schuliga, J. Read and D. A. Knight, *Ageing Res. Rev.*, 2021, **70**, 101405.
76 S. Wang, D. Xiang, F. Tian and M. Ni, *J. Med. Microbiol.*, 2021, **70**, 001352.
77 Y. Guan, M. Zhang, J. Song, M. Negrete, T. Adcock, R. Kandel, L. Racioppi and S. Gerecht, *Adv. Sci.*, 2025, 2417778.
78 H. Du, J. M. Bartleson, S. Butenko, V. Alonso, W. F. Liu, D. A. Winer and M. J. Butte, *Nat. Rev. Immunol.*, 2023, **23**, 174–188.
79 M. L. Meizlish, Y. Kimura, S. D. Pope, R. Matta, C. Kim, N. H. Philip, L. Meyaard, A. Gonzalez and R. Medzhitov, *Sci. Adv.*, 2024, **10**, eadk6906.
80 J. Yu, F. Chen, X. Wang, N. Dong, C. Lu, G. Yang and Z. Chen, *Polym. Degrad. Stab.*, 2016, **133**, 312–320.
81 L. E. Jansen, L. J. Negrón-Piñeiro, S. Galarza and S. R. Peyton, *Acta Biomater.*, 2018, **70**, 120–128.
82 N. J. Darling, Y.-S. Hung, S. Sharma and T. Segura, *Biomaterials*, 2016, **101**, 199–206.
83 E. A. Phelps, N. O. Enemchukwu, V. F. Fiore, J. C. Sy, N. Murthy, T. A. Sulchek, T. H. Barker and A. J. García, *Adv. Mater.*, 2012, **24**, 64–70, 62.
84 K. Xu, D. A. Cantu, Y. Fu, J. Kim, X. Zheng, P. Hematti and W. J. Kao, *Acta Biomater.*, 2013, **9**, 8802–8814.
85 E. Y. Du, M. Jung, J. Skhinas, M. K. Tolentino, N. Jamshidi, J. Houng, K. C. Tjandra, M. Engel, R. Utama and R. Tilley, *bioRxiv*, 2022, 2022.2010.2006.511222, DOI: 10.1101/2022.2010.2006.511222.
86 H. Mahmodi, A. Piloni, R. Utama and I. Kabakova, *bioRxiv*, 2021, 2021.2002.2018.431535. DOI: 10.1101/2021.02.18.431535.
87 U. Kolbe, B. Yi, T. Poth, A. Saunders, S. Boutin and A. H. Dalpke, *Front. Immunol.*, 2020, **11**, 598636.
88 C. Ma, X. Ma, B. Jiang, H. Pan, X. Liao, L. Zhang, W. Li, Y. Luo, Z. Shen, X. Cheng, M. Lian and Z. Wang, *Signal Transduction Targeted Ther.*, 2021, **6**, 353.
89 A. Schoeniger, S. Adolph, H. Fuhrmann and J. Schumann, *Int. J. Mol. Sci.*, 2011, **12**, 7510–7528.
90 R. Chen, D. Yang, L. Shen, J. Fang, R. Khan and D. Liu, *Immun., Inflammation Dis.*, 2022, **10**, e740.
91 Q. Deng, Y. Wang, Y. Zhang, M. Li, D. Li, X. Huang, Y. Wu, J. Pu and M. Wu, *Infect. Immun.*, 2016, **84**, 56–66.
92 B. A. Al-lateef, M. S. M. Al-shukri and M. R. Judi, *Med. J. Babylon*, 2023, **20**, 201–205.
93 F. Bastaert, S. Kheir, V. Saint-Criq, B. Villeret, P. M.-C. Dang, J. El-Benna, J.-C. Sirard, R. Voulhoux and J.-M. Sallenave, *Front. Immunol.*, 2018, **9**, 01675.
94 L. Zhang, Y. Wang, G. Wu, W. Xiong, W. Gu and C.-Y. Wang, *Respir. Res.*, 2018, **19**, 170.
95 L. Deng, Z. Jian, T. Xu, F. Li, H. Deng, Y. Zhou, S. Lai, Z. Xu and L. Zhu, *Molecules*, 2023, **28**, 28052379.
96 A. M. Keestra-Gounder and P. E. Nagao, *Front. Immunol.*, 2023, **14**, 1075834.
97 N. Cole, M. Krockenberger, S. Bao, K. W. Beagley, A. J. Husband and M. Willcox, *Infect. Immun.*, 2001, **69**, 4116–4119.
98 N. S. Gonçalves, M. Ghaem-Maghami, G. Monteleone, G. Frankel, G. Dougan, D. J. Lewis, C. P. Simmons and T. T. MacDonald, *Infect. Immun.*, 2001, **69**, 6651–6659.
99 G. van Loo and M. J. M. Bertrand, *Nat. Rev. Immunol.*, 2023, **23**, 289–303.
100 S. Zhao, J. Jiang, Y. Jing, W. Liu, X. Yang, X. Hou, L. Gao and L. Wei, *Cell Death Dis.*, 2020, **11**, 70.
101 G. D. Kalliolias and L. B. Ivashkiv, *Nat. Rev. Rheumatol.*, 2016, **12**, 49–62.
102 Y. Chuang, M. E. Hung, B. K. Cangelose and J. N. Leonard, *Innate Immun.*, 2016, **22**, 647–657.
103 R. Lv, Q. Bao and Y. Li, *Mol. Med. Rep.*, 2017, **16**, 9111–9119.
104 C. J. Hastings, G. E. Himmler, A. Patel and C. N. H. Marques, *mBio*, 2023, **14**, e0005623.
105 T. Sawa, D. B. Corry, M. A. Gropper, M. Ohara, K. Kurahashi and J. P. Wiener-Kronish, *J. Immunol.*, 1997, **159**, 2858–2866.
106 V. A. Belo, J. A. Pereira, S. F. D. Souza, F. d. L. Tana, B. P. Pereira, D. d. O. Lopes, C. S. Ceron, R. D. Novaes, P. P. Corsetti and L. A. de Almeida, *Cell Tissue Res.*, 2021, **383**, 1123–1133.
107 V. Barbarin, Z. Xing, M. Delos, D. Lison and F. Huaux, *Am. J. Physiol.: Lung Cell. Mol. Physiol.*, 2005, **288**, L841–L848.

108 L. Sun, M. C. Louie, K. M. Vannella, C. A. Wilke, A. M. LeVine, B. B. Moore and T. P. Shanley, *Am. J. Physiol.: Lung Cell. Mol. Physiol.*, 2011, **300**, L341–L353.
109 A. Bhattacharyya, K. Boostanpour, M. Bouzidi, L. Magee, T. Y. Chen, R. Wolters, P. Torre, S. K. Pillai and M. Bhattacharya, *Am. J. Physiol.: Lung Cell. Mol. Physiol.*, 2022, **322**, L495–L502.
110 S. Almansour, J. L. Dunster, J. J. Crofts and M. R. Nelson, *Math. Biosci.*, 2024, **377**, 109289.
111 A. Garcia-Sabaté, W. K. E. Mohamed, J. Sapudom, A. Alatoom, L. Al Safadi and J. C. M. Teo, *Bioengineering*, 2020, **7**, 7030113.
112 R. Mittal, S. Sharma, S. Chhibber and K. Harjai, *Comp. Immunol., Microbiol. Infect. Dis.*, 2006, **29**, 12–26.
113 S. Bhusari, S. Sankaran and A. del Campo, *Adv. Sci.*, 2022, **9**, 2106026.
114 L. Wang, Y. C. Wong, J. M. Correira, M. Wancura, C. J. Geiger, S. S. Webster, B. J. Butler, G. A. O'Toole, R. M. Langford, K. A. Brown, B. Dortdivanlioglu, L. Webb, E. Cosgriff-Hernandez and V. D. Gordon, *bioRxiv*, 2023, DOI: 10.1101/2023.01.26.525810.
115 K. W. Kolewe, J. Zhu, N. R. Mako, S. S. Nonnenmann and J. D. Schiffman, *ACS Appl. Mater. Interfaces*, 2018, **10**, 2275–2281.